JOURNAL OF GEOPHYSICAL RESEARCH, VOL. 113, D16305, doi:10.1029/2007JD008657, 2008

Size-resolved chemical composition of aerosol particles during a monsoonal transition period over the Indian Ocean

M. T. Spencer,[1] J. C. Holecek,[2] C. E. Corrigan,[2] V. Ramanathan,[2] and K. A. Prather[1,3]

Received 14 March 2007; revised 10 November 2007; accepted 6 December 2007; published 21 August 2008.

[1] An aerosol time-of-flight mass spectrometer (ATOFMS) was used to measure the size-resolved mixing state of particles over the northern Indian Ocean in October and November 2004. This period was chosen to observe the impact of the monsoonal transition on the size, chemistry, sources, and radiative properties of atmospheric aerosols in the region. Overall, elemental carbon with sulfate (EC-sulfate), biomass/biofuel burning, fresh sea salt (SS), aged sea salt, fly ash, and EC mixed with sea salt were the dominant supermicron particle types, whereas EC-sulfate, biomass/biofuel burning, and fly ash were the dominant submicron particle types. Interestingly, particles composed mostly of aged organic carbon and nitrate were virtually absent during the campaign. This is possibly from low ozone formation in the region or selective scavenging during transport. Notably, during long-range transport periods when an aethalometer measured the highest black carbon concentrations, 77% of submicron particles between 0.5 and 2.5 μm and 71% of EC/soot particles contained an intense $^{39}K^{+}$ ion (a known tracer for biomass/biofuel combustion). These observations suggest when the air mass originated from India, biofuel combustion represented a significant source of the regional atmospheric brown cloud. The majority ($\sim$80%) of EC and biomass/biofuel burning particles were mixed with significant amounts of sulfate due to extensive secondary processing of these particles during transport. EC mixed with sea salt was also observed suggesting the particles had undergone cloud processing and become internally mixed during transport. These measurements support the use of an internal mixture of sulfate with EC/soot and biomass/biofuel burning in models to accurately calculate radiative forcing by aerosols in this region.

Citation: Spencer, M. T., J. C. Holecek, C. E. Corrigan, V. Ramanathan, and K. A. Prather (2008), Size-resolved chemical composition of aerosol particles during a monsoonal transition period over the Indian Ocean, *J. Geophys. Res.*, *113*, D16305, doi:10.1029/2007JD008657.

1. Introduction

[2] Predicting the effect of air pollution on climate change is critical for hedging increasing world economic growth with environmental impacts from rising global air pollution. Large uncertainties still remain in accurately predicting the effects aerosol particles have on the hydrological cycle, direct and indirect radiative forcing, and overall climate change [*Chen and Penner*, 2005; *Intergovernmental Panel on Climate Change* (*IPCC*), 2001; *Knutti et al.*, 2002; *Lohmann and Feichter*, 2005; *Morgan et al.*, 2006; *Ramanathan et al.*, 2005]. A large fraction of this uncertainty stems from limited information on the chemical composition and mixing state of particles in the atmosphere [*Chandra et al.*, 2004; *IPCC*, 2001; *Jacobson*, 2001; *Lohmann and Feichter*, 2005; *Myhre et al.*, 2004; *Schwartz*, 2004]. As an air mass ages, changes in particle chemical composition and mixing state further complicate predicting the impact of aerosols on climate. Sulfate can decrease atmospheric absorption by increasing the hydrophilic nature of soot particles, thus increasing their wet removal rate [*Stier et al.*, 2006]. Many research groups, including most recently Stier et al., have shown that internally mixed elemental carbon-sulfate particles will increase atmospheric absorption by increasing a particle's absorption efficiency [*Stier et al.*, 2006]. To quantify the direct climate forcing of aerosol particles, it is essential to understand the dynamic nature of particle chemical composition and mixing state.

[3] Project Atmospheric Brown Cloud (ABC) was designed to monitor changes in aerosol chemical composition, optical depth, radiative forcing and cloud properties within the Indo-Asian and Pacific regions (http://www-abc-asia.ucsd.edu/). The goals of the ABC project involve using data collected from climate observatories for input into climate models to help increase their predictive power and

[1]Department of Chemistry and Biochemistry, University of California, San Diego, La Jolla, California, USA.
[2]Center for Atmospheric Sciences, Scripps Institution of Oceanography, University of California, San Diego, La Jolla, California, USA.
[3]Also at Center for Atmospheric Sciences, Scripps Institution of Oceanography, University of California, San Diego, La Jolla, California, USA.

0148-0227/08/2007JD008657$09.00

better understand the environmental impact of rising air pollution on regional and global scales. Specifically, ABC aims to address the significance of environmental changes due to rising air pollution in the Indo-Asian and Pacific region. Climate observatories are being operated on a long-term basis (2004–2008), with intermittent intense aerosol characterization periods at selected observatory sites. This paper describes measurements made at the first operational ABC climate observatory, which lies in the northern Indian Ocean on Hanimaadhoo Island, Republic of Maldives. The northern Indian Ocean experiences an annual monsoonal transition in the month of October. This transition period is characterized by a shift in regional wind pattern from a southwesterly to a northeasterly flow [*Kripalani and Kumar*, 2004]. During the transition period, the regional air mass fluctuates until the dry monsoon period when there is a dominant northeasterly flow [*Ramana and Ramanathan*, 2006]. This northeasterly flow carries air pollution from Asia over the relatively unpolluted Indian Ocean [*Guazzotti et al.*, 2001, 2003; *Neusüß et al.*, 2002; *Quinn et al.*, 2002; *Reiner et al.*, 2001]. Thus the transition period offers a unique opportunity to monitor and compare aerosol physical/chemical properties, cloud physical/chemical properties and radiation flux, as air pollution is transported into the unpolluted North Indian Ocean. The ABC Post Monsoonal Experiment (APMEX) was an intensive aerosol characterization experiment that took place during this transition period (15 October to 5 November 2004) at the Republic of Maldives Climate Observatory on Hanimaadhoo Island (MCOH).

[4] During APMEX, an aerosol time-of-flight mass spectrometer (ATOFMS), aethalometer, nephelometer, aerosol particle sizer (APS), scanning mobility particle sizer (SMPS), and a suite of solar radiation instrumentation were operated at MCOH [*Corrigan et al.*, 2006; *Ramana and Ramanathan*, 2006]. This paper focuses on results obtained with an ATOFMS during APMEX. A more detailed discussion of other instrumentation operated during the APMEX campaign has been published elsewhere [*Corrigan et al.*, 2006; *Ramana and Ramanathan*, 2006].

[5] The ATOFMS used in this study measures the aerodynamic size (0.3–2.5 μm) and chemical composition of individual particles in real time. A general discussion of the particle chemical composition and mixing state during the campaign is presented along with a discussion of the air mass back trajectories used to identify particle source locations. The trajectories are then correlated with the temporal evolution of the chemically different particle types observed for the duration of the study. In future work, these results will be combined with solar radiation measurements to help advance our understanding of the major sources and processes contributing to the aerosol radiative forcing in this region of the world.

2. Experimental Section

2.1. Location

[6] Measurements were made from 15 October 2004 through 5 November 2004 on the island of Hanimaadhoo (6.776°N, 73.183°E), Republic of Maldives. Hanimaadhoo Island is approximately 4 km (north-south) by 1 km (east-west) in size. There are approximately 1200 residents on the island. The MCOH observatory is located at the northern tip of the island where the prevailing winds come from over the ocean. The majority of the island's residents live approximately 2 km south of the observatory; therefore local pollution sources are minimal.

2.2. Aerosol Characterization Instrumentation

[7] Ambient aerosol particles were sampled from a 15 m high, 20 cm diameter sampling mast with laminar flow. The sampling mast entered a temperature controlled room in the MCOH. This room was kept at ambient temperature to sample particles at ambient relative humidity (RH) and prevent condensation or evaporation during particle measurements. Aerodynamic particle sizer (TSI model 3321), mobility particle sizer (TSI model 3936), total particle counter (TSI CPC-3022), aethalometer (Magee Scientific), and nephelometer instruments (TSI integrating nephelometer model 3563) were located within the ambient temperature room. A more detailed description of the MCOH observatory has been published previously [*Corrigan et al.*, 2006]. The ATOFMS was located in an air conditioned room adjacent to the ambient temperature room. A 1-m-long piece of insulated sampling line was used between the ambient temperature sampling mast and the ATOFMS. Particle losses due to gravitational settling during transport from the exit of the sampling mast to the ATOFMS were estimated to be less than 5% for 2.5 μm particles with a density of 1.0 g·cm^{-3}.

[8] Filter based samples were collected at the top of the 15 m tower every 24 h. A detailed discussion of the methods used and overall results for the filter based data is given by *Stone et al.* [2007]. The nephelometer data was corrected for truncation errors and other measurement errors using the method outlined by *Anderson and Ogren* [1998]. The black carbon and absorption data obtained from the aethalometer were corrected using the approach presented by *Arnott et al.* [2005].

[9] The aerodynamic size and chemical composition of individual particles (0.3–3.0 μm) was measured using a transportable aerosol time-of-flight mass spectrometer (ATOFMS). A detailed description of the ATOFMS has been published previously and only a brief description is given here [*Gard et al.*, 1997; *Prather et al.*, 1994]. Aerosol enters into the vacuum pumped ATOFMS through a converging nozzle inlet at a flow of ~0.96 lpm. Upon entering the ATOFMS, the air flow undergoes a supersonic expansion due to a drop in pressure from ~760 to ~3 Torr. This gas expansion accelerates particles to a terminal velocity based on the aerodynamic size of each particle (smaller particles are accelerated to a faster terminal velocity). After this acceleration, particles pass through two skimmers where a large portion of gas molecules are pumped away. Particles then pass through two vertically separated (6 cm) continuous wave (CW) lasers. Light scattered by each particle as it passes through the CW lasers is detected with a photomultiplier tube (PMT). The difference in time between the two PMT signals is used to measure the velocity of the particle, and ultimately the aerodynamic size. The measured particle velocity is then used to calculate the precise time the particle is within the ion source region of a dual polarity time-of-flight mass spectrometer. At the precise time when the particle enters the ion source region, a Q-switched Nd:YAG laser operated at λ = 266 nm with an

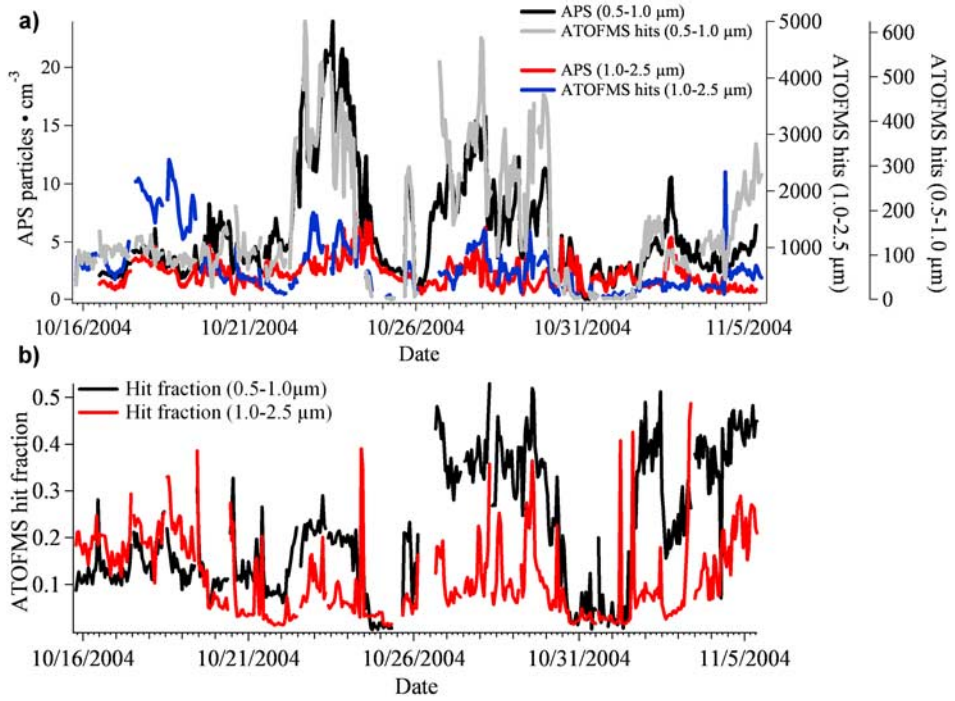

Figure 1. (a) Comparison of the number of particles between 0.5–2.5 μm analyzed (hit) using ATOFMS (left *y* axis) and the number of particles per cubic centimeter measured using an APS (right *y* axis) for the duration of the APMEX field campaign (*x* axis). (b) The percent of ATOFMS hit particles (Hits/Hits+Miss) for the duration of the APMEX field campaign.

8 ns pulse length and 400 μm spot diameter is fired at the particle. Positive and negative ions formed from laser ablation/ionization of the particle are detected using a dual ion time-of-flight mass spectrometer. When a mass spectrum is generated from a particle, it is designated as being "hit." When a particle is sized by the ATOFMS but there is not a mass spectrum generated for that particle, it is considered "missed."

2.3. Data Analysis

[10] ATOFMS data were imported into Matlab 6.5.1 (The Math Works, Inc.) using YAADA version 1.2 (http://www.yaada.org). Portions of the YAADA toolkit were also used for data analysis. Particle chemical classes were derived by clustering individual particle mass spectra together using an Adaptive Resonance Theory neural network (ART-2a) [*Hopke and Song*, 1997; *Song et al.*, 1999]. Similarities between individual mass spectra (using the presence and intensity of ion peaks) are calculated using ART-2a. Mass spectra that have a similarity above a set threshold (vigilance factor) are clustered together and considered chemically similar. The ART-2a parameters used for chemical classification were: learning rate = 0.05, vigilance factor = 0.85 and iterations = 20. Approximately 380,000 unique particle mass spectra were analyzed using ART-2a which yielded ~320 unique clusters. The 60 most populated clusters represent over 92% of the mass spectra from the study and thus were used for the results presented in this paper. The other 8% of clusters are made up of a majority of miscalibrated mass spectra and a small number of particles that generated unique mass spectra. Although these 60 clusters are considered unique in the ART-2a analysis, many of the clusters exhibit a similar dominant ion pattern when compared to other clusters by visual inspection. For example, it is common to find numerous clusters that consist of mass spectra with dominant elemental carbon ions (12[$C^{+/-}$], 24[$C_2^{+/-}$]. . . .$C_n^{+/-}$) and an intense −97[HSO_4^-]. Small differences in peak ratios or a miscalibrated peak lead to particles with these signatures being placed in separate ART-2a clusters [*Rebotier and Prather*, 2007]. The goal of this paper is to show the major general particle types; thus, clusters with the same peaks in slightly varying proportions are grouped into the same chemical class. Using this method, the top 60 clusters were refined into 8 chemical classes.

[11] Relative area matrices are created by normalizing each mass spectrum to the most intense ion peak in the spectrum and then averaging together all normalized individual mass spectra within the cluster. In general, the relative area matrix resembles an individual particle mass spectrum within a given particle class.

3. Results and Discussion

[12] A comparison of the number of ATOFMS hit particles (0.3–2.5 μm diameter) versus the particle number concentration measured with an APS (0.5–2.5 μm diameter) can be used to determine whether the relative particles counts of the ATOFMS track the relative particle counts of the APS. Figure 1 shows the time series of ATOFMS particle counts (hit particles only) and the APS particle number concentration (particles/cubic centimeter) with 1 h time resolution. In general, the ATOFMS particle counts are correlated with the APS particle concentrations throughout the study, however there are a few notable exceptions. From 16–20 October, the ATOFMS detected a relatively high number of particles, and on 22 October, 27 October,

and 2–3 November the APS shows a sharp spike in particle concentrations while the ATOFMS counts did not show these increases. Excluding these few periods, a correlation between the APS and ATOFMS hit particles (0.5–2.5 μm) gives an $R^2 \sim 0.52$.

[13] Figure 1b shows the ATOFMS hit fraction for all particles that generated a mass spectrum for the duration of the APMEX field campaign. During APMEX the hit fraction fluctuated between ~0.05–0.25 for supermicron particles and ~0.05–0.40 for submicron particles. In general, the submicron particles showed reasonable stability, particularly during high concentration periods. Notably, an increase in the overall hit fraction for submicron particles occurred on 26 October. This was due to an improvement in the alignment of the scattering lasers during a "down-time" on 25 October. The submicron hit fraction increased to approximately 0.35 (or 35%). Fluctuations in the hit fraction can reflect changes in the chemical composition of different particle types. Comparing the hit fraction to the APS number concentration shows those periods when the hit fraction was lowest correspond to periods when the APS concentrations were also low. As will be shown later, during the low concentration periods there was a dominant percentage of wet fresh sea salt particles. During the high particle concentration periods, there was generally an increase in the hit fraction along with a larger percentage of elemental carbon with sulfate and biomass/biofuel burning particle types. These EC and biomass/biofuel burning particle types are usually strongly absorbing and thus very detectable by the ATOFMS LDI process. Fresh wet sea salt is undercounted by as much as 6 times compared to elemental carbon and biomass/biofuel with the ATOFMS. We have shown in other studies in marine environments this negative bias can be reduced by drying the aerosol or controlling the relative humidity before it enters the ATOFMS. However, during this study no conditioning was done to the aerosol before it entered the ATOFMS and thus the biases were very apparent, especially during clean marine condition periods. As discussed later, these and other biases must be taken into account when scaling the ATOFMS data [*Wenzel et al.*, 2003].

[14] During other bias periods on 22 October, 27 October, and 2–3 November, the APS shows a spike in particle number concentrations while the ATOFMS shows a decrease in hit percentage of particles. As will be shown later, during this period, aethalometer absorption measurements decrease while the scattering coefficient (b_{sp}) increases as measured with a nephelometer. The number of particle scatters measured with the ATOFMS, particles which are sized but do not produce mass spectra, track the nephelometer data (not shown). The coupled increase in the scattering coefficient and number of ATOFMS scatters, along with a subsequent decrease in the absorptivity of the aerosol and fraction of ATOFMS hit particles indicates the presence of a "missed" particle type. Wenzel et al. observed a missed particle type using ATOFMS in Atlanta Georgia and through comparison with other measurements concluded the particles to be composed of pure ammonium sulfate [*Wenzel et al.*, 2003]. Ammonium sulfate is strong scatterer but does not absorb laser radiation from the ionization laser (266 nm), thus the ATOFMS is not as sensitive to ammonium sulfate particles and does not detect them as efficiently as other particle types [*Thomson et al.*, 1997]. Wenzel et al. also observed that the missed particles became increasingly abundant in the smallest detectable size range of the ATOFMS used in that study (between 0.3–0.5 μm). However, the missed particle types during APMEX were observed across a much broader size range (0.6–2.0 μm), with the lowest hit percentage between ~1.0–1.5 μm. We can only speculate on the composition of the missed particles during these time periods, but we do know they did not absorb UV light and had a broad size distribution extending up into the supermicron size range. Because of the larger size of the missed particle type, they could have been wet sea salt. They also could have been ammonium sulfate, however this is the only study where nominally pure sulfate particles would have been observed in these larger sizes, but not small sizes. A source or formation mechanism that would form large pure sulfate particles and not small ones is difficult to envision. For the vast majority of the study, the ATOFMS shows submicron sulfate mixed with biomass/biofuel and EC/soot particles.

3.1. Chemical Composition

[15] Eight major particle types were observed during the APMEX field campaign: fresh sea salt (fresh-SS), aged sea salt (aged-SS), elemental carbon with sea salt (EC-SS), elemental carbon with sulfate (EC-sulfate), fly ash, potassium-biomass (biomass/biofuel burning), organic carbon (OC), and calcium-dust (Ca-dust). An area matrix for each of these particle types is given in Figure 2 and a brief description of each type follows. Fresh-SS is characterized by ion peaks for $^{23}Na^+$, 81/83[Na_2Cl^+], and −35/−37[Cl^-]. In addition to the major peaks in fresh-SS, aged-SS contains intense ions at −46[NO_2^-] and −62[NO_3^-]. EC-SS has sea salt marker ions and also carbon cluster ions 12[$C^{+/-}$], 24[$C_2^{+/-}$]....$C_n^{+/-}$. EC-sulfate contains dual polarity carbon cluster ions (12[$C^{+/-}$], 24[$C_2^{+/-}$]....$C_n^{+/-}$), a smaller $^{39}K^+$ peak as well as an intense peak for sulfate −97[HSO_4^-]. Fly ash is characterized by ion peaks for $^{39}K^+$ along with $^7Li^+$, $^{23}Na^+$, $^{27}Al^+$, −46[NO_2^-], −62[NO_3^-], and −35/−37[Cl^-] [*Suess*, 2002]. Biomass/biofuel burning particles show intense $^{39}K^+$ and −97[HSO_4^-] ions, as well as less intense OC marker ions such as 15[CH_3^+], 27[$C_2H_3^+$], 29[$C_2H_5^+$], 43[$C_2H_3O^+$], and EC marker ions (12[$C^{+/-}$], 24[$C_2^{+/-}$]....$C_n^{+/-}$) [*Silva et al.*, 1999]. The biomass burning particle class is a mixture of EC and OC. The OC particle class is characterized by OC marker ions: 15[CH_3^+], 27[$C_2H_3^+$], 29[$C_2H_5^+$], 37[C_3H^+], and 43[$C_2H_3O^+$] and ions at +77 and +91 which are generally attributed to fragment ions from phenyl-alkyl compounds; no negative ions were detected for this OC particle class. The peak at 19[H_3O^+] and the lack of negative ions provide evidence that the OC particles also contained water and other secondary species. Ca-dust is characterized by an intense m/z 40 [Ca^+], as well as 57[$CaOH^+$], 96[Ca_2O^+], −17[OH^-], −35/37[Cl^-], −42[CNO^-] and −46[NO_2^-].

[16] The sulfate ion at m/z −97 [HSO_4^-], observed mixed with EC and biomass/biofuel particle types discussed above, was much more intense than in previous ATOFMS combustion source characterization studies [*Silva et al.*, 1999; *Sodeman et al.*, 2005; *Toner et al.*, 2006]. This intense sulfate ion signal suggests these particles have undergone significant secondary processing during transport. Previous

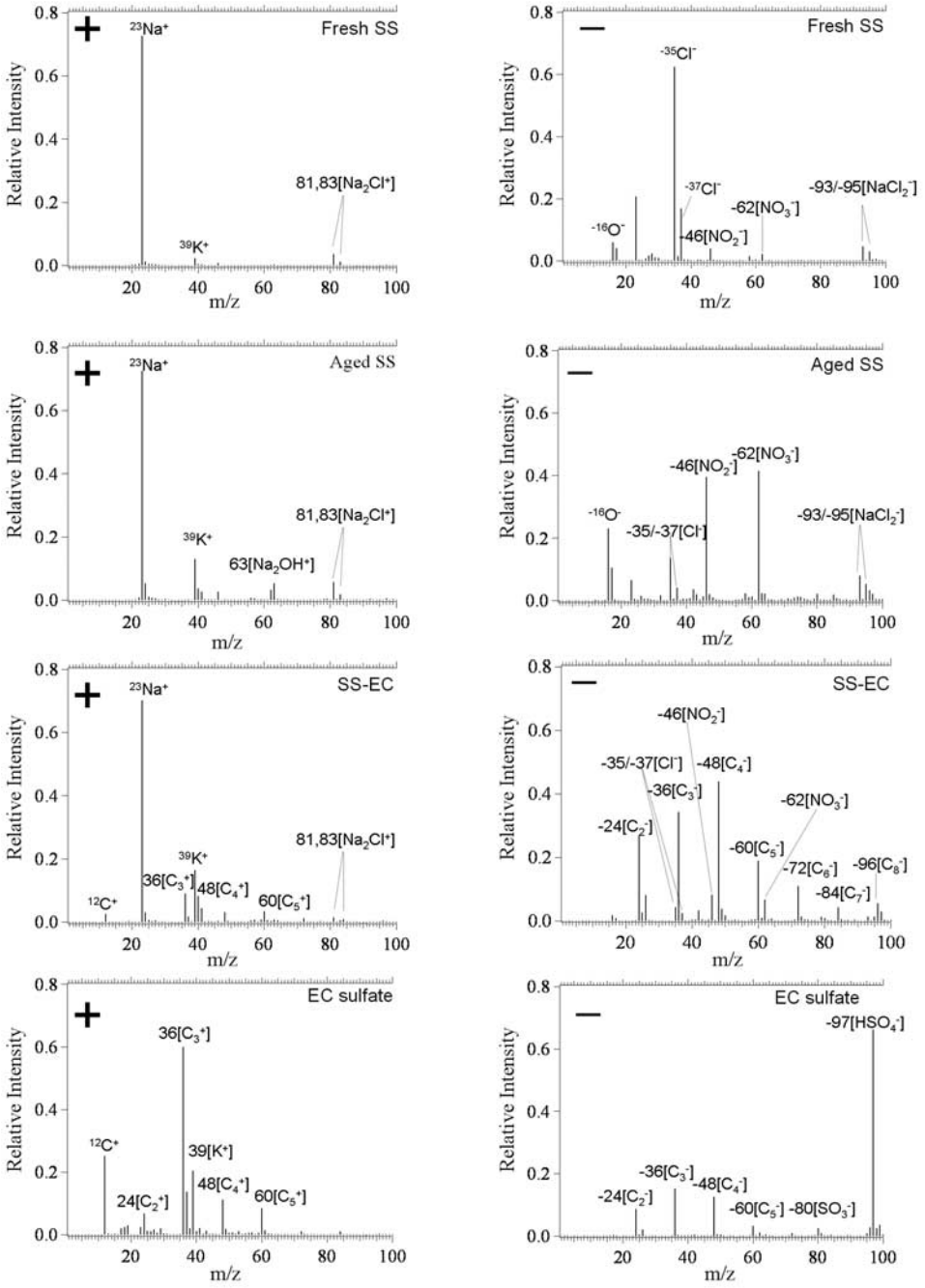

Figure 2. Area matrices for the top eight particle classes (fresh-SS, aged-SS, EC-SS, EC-sulfate, fly ash, biomass/biofuel burning, OC and Ca-dust) observed during APMEX.

studies have shown that aerosols become internally mixed as they get further from the source [*Clarke et al.*, 2004]. Our results are consistent with this as we detect EC/biomass burning and sulfate as internal mixtures far from the source. EC mixed with sulfate was also observed during INDOEX and has been observed over the midlatitudes of the North Pacific Ocean [*Alfaro et al.*, 2003; *Kaneyasu and Murayama*, 2000; *Neusüß et al.*, 2002]. The presence of EC and sea salt within the same particle (EC-SS) suggests these particles have undergone coagulation most likely during cloud processing to become a mixed particle type. EC mixed with NaCl has been shown to act as an effective cloud condensation nuclei (CCN) [*Dusek et al.*, 2006]. Light absorption by sulfate-coated or organic carbon-coated EC particles (EC core surrounded by sulfate or organic shell) has been shown to be 2–4 times higher then uncoated EC [*Bond et al.*, 2006; *Fuller et al.*, 1999; *Jacobson*, 2001; *Schnaiter et al.*, 2005]. Furthermore, during INDOEX, Neusüß et al. observed an increase in the absorption efficiency with decreasing EC mass fraction and attributed this to increasing amounts of light scattering material on the EC particles [*Neusüß et al.*, 2002]. The EC-sulfate, biomass/biofuel burning, and EC-SS particles described above could have this core-shell structure; however, this cannot be

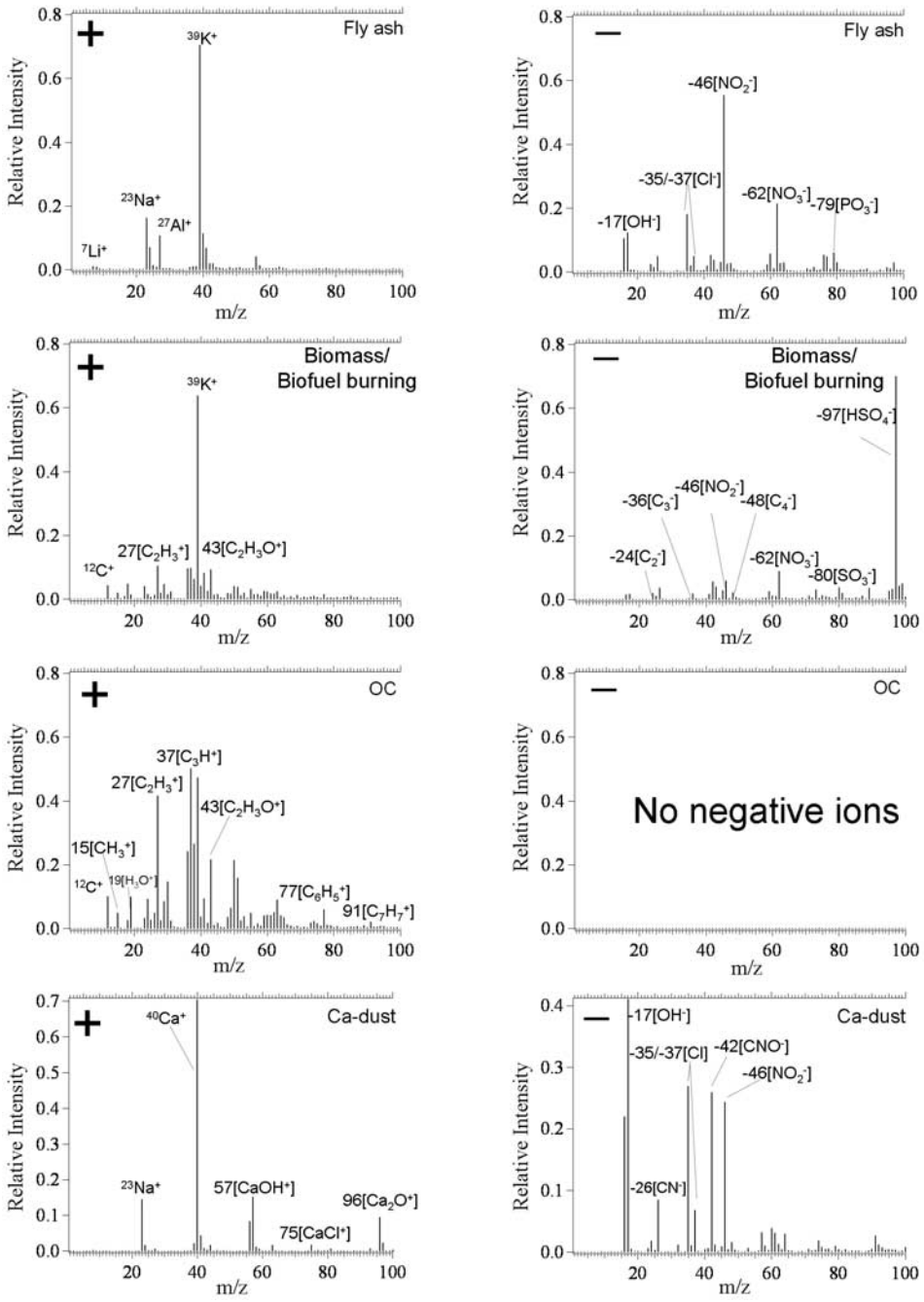

Figure 2. (continued)

definitively determined with the current data set. Complementary single particle measurements using techniques such as scanning electron microscopy might be able to help determine the actual physical state of these mixed particles. Simultaneous measurements of particle density and shape would also help unravel the physical state of these particles [*Moffet and Prather*, 2005; *Spencer et al.*, 2007].

[17] Organic carbon and nitrate are two species which are commonly detected with ATOFMS in other regions of the world. Nominally pure OC, OC mixed with EC, and particles containing significant amounts of nitrate were virtually absent (compared to other ATOFMS field campaigns) during APMEX. Filter based measurements also showed a low abundance of nitrate [*Stone et al.*, 2007]. As will be discussed later, much of the black carbon, sulfate, and biomass/biofuel burning measured during APMEX originated from India. Dickerson et al. have shown that due to the large number of two stroke engines used in India, there is a large atmospheric VOC/NO_x ratio (220 ppm carbon/ppm NO_x) [*Dickerson et al.*, 2002]. The large amount of VOC and small amount of NO_x emitted from 2 stroke engines leads to NO_x limited ozone formation, and thus there is only modest amounts of ozone formed and lower levels of NO_x compared to concentrations normally encountered in western cities. Ozone concentrations have also been shown to be lower in the month of October in

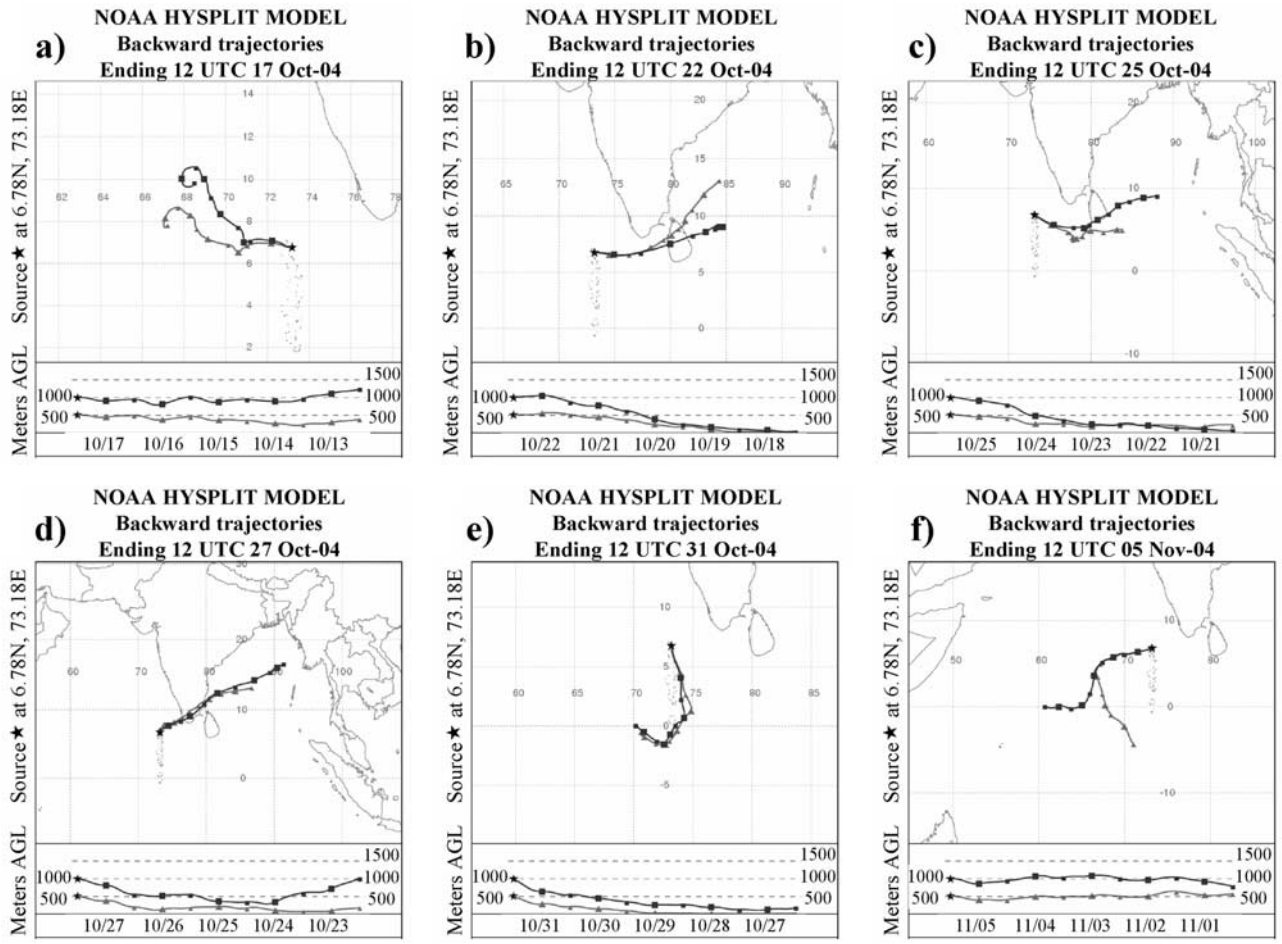

Figure 3. HYSPLIT back trajectories for six time periods during the APMEX campaign. (a) 17 October 2004, (b) 22 October 2004, (c) 25 October 2004, (d) 27 October 2004, (e) 31 October 2004, and (f) 5 November 2004.

rural southeast India [*Debaje et al.*, 2003], and in general rarely exceed 100 ppb in the north Indian Ocean [*Lal et al.*, 2000; *Stehr et al.*, 2002]. These lower ozone concentrations could lead to less oxidation of VOCs and hence less secondary organic material condensing on primary particles such as EC before they are transported over the Indian Ocean. Furthermore, particles containing organic material and nitrate are possibly scavenged by clouds and rain during transport over the Indian Ocean. It should be noted that filter based methods did measure a significant fraction of PM < 2.5 μm OC (average $\sim$ 0.6 $\mu g \cdot m^{-3}$). It is likely that most of the filter-OC was a mixture of biomass/biofuel and marine aerosols. ATOFMS organic carbon ion signals are suppressed by intense inorganic ions such as Na and K generated from sea salt and biomass/biofuel burning particles during laser ionization and thus organic material in these particle types are masked by the inorganic ions. Future ATOFMS measurements in a southern India metropolitan area would be very useful to compare the differences between the primary sources and the chemically transformed particles measured at MCOH.

3.2. Temporal Trends

[18] Figure 3 shows HYSPLIT five day air mass back trajectories (500 and 1000 m above ground level) representative of six distinct time periods when the particle chemical class fractions changed (see http://www.arl.noaa.gov/ready/hysplit4.html). During these six different time periods, changes in the air mass back trajectories corresponded with changes in the chemical mixing state of the single particles. In Figure 3a, the HYSPLIT model shows the air mass coming from the west-northwest (long-range transport–Arabian Sea) on 17 October 2004. Figures 3b and 3d show that on 22 October 2004 and 27 October 2004 the air mass originated from the east-northeast (southern India/Sri Lanka). Figure 3c shows the air mass was coming from the east-southeast (Indian Ocean/southern Sri Lanka) on 25 October 2004. Figure 3e shows the air mass was coming from the south (Indian Ocean/Maldives) on 31 October 2004. Figure 3f shows the air mass was coming from the west-southwest (Indian Ocean) on 5 November 2004.

[19] Figure 4a shows the supermicron (1.0–2.5 μm) time series of the fractions of different particle classes described above. It should be noted that Figure 4a has not been adjusted for any sampling bias and represents the raw ATOFMS data. Note that $\sim$10% of the hit particles were unclassified and are made up of some miscalibrated particles and small numbers of particles that generated unique looking mass spectra. Figure 4a shows the six distinct periods when there were significant differences in the

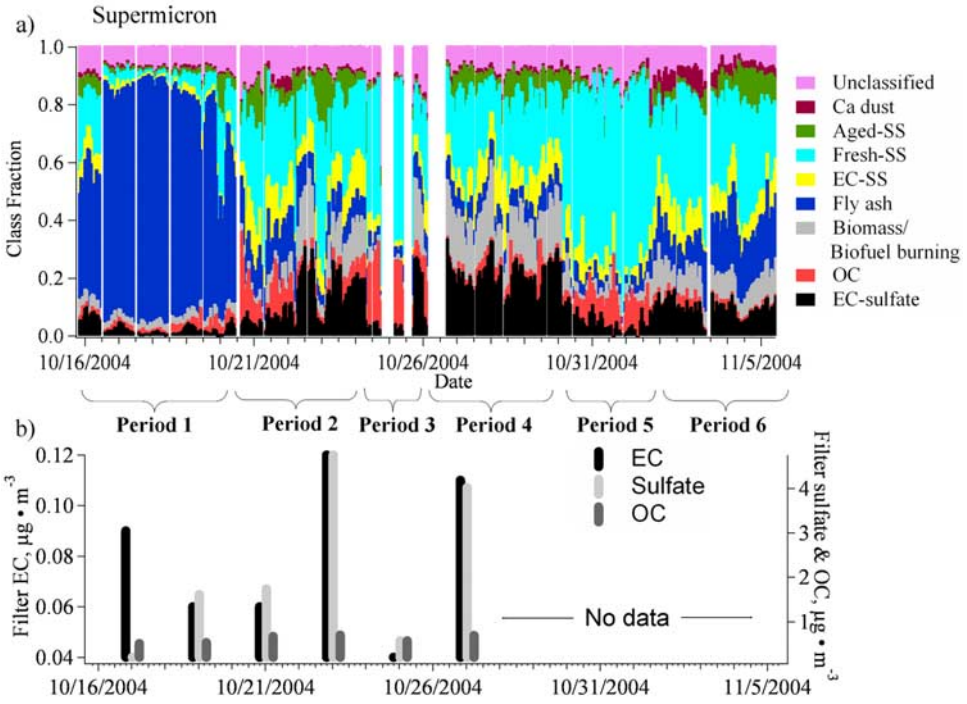

Figure 4. (a) The unscaled fraction of different supermicron particle chemical classes in 1 h time resolution for the duration of the APMEX field campaign. (b) Mass of EC, sulfate and OC per cubic meter as determined by 24 h filter measurements during APMEX.

chemistry of the supermicron sized particles; from 15–20 October (period 1), 20–24 October (period 2), 24–26 October (period 3), 26–30 October (period 4), 30 October to 2 November (period 5) and 2–5 November (period 6). During period 1, the site was impacted by a dominant fraction of supermicron fly ash particles. The presence of fly ash during this period is supported by an increase in the mass of different metals known to exist in fly ash (Al, Mn, Li, Fe, Ti, V, Cr) [*Vijayan et al.*, 1997; *Zhang et al.*, 2005] measured on filters [*Stone et al.*, 2007]. A possible source for these fly ash particles could be incineration or coal combustion. The fly ash does not resemble biomass/biofuel burning or vehicle exhaust particles that have been measured in previous ATOFMS source characterization studies. As discussed in Guazzotti et al., the mass spectral signature resembles fly ash particles formed by coal combustion [*Guazzotti et al.*, 2003; *Suess*, 2002]. In particular, the Li^+ ion signal was observed in 55% of the supermicron particle spectra during period 1. Similar to a previous ATOFMS study conducted by Guazzotti et al. during INDOEX, this signature was mainly detected when there was extensive transport from the Arabian peninsula [*Guazzotti et al.*, 2003].

[20] When the air mass comes from heavily populated areas near India and Sri Lanka to the east-northeast (periods 2 and 4), the relative contributions of EC-sulfate, OC, biomass/biofuel burning, fresh-SS, and EC-SS particle types increase substantially with a significant decrease in Li-containing fly ash particles. During periods 2 and 4, there is also a corresponding increase in the fraction of submicron particles. When the air mass comes from the east or south (periods 3 and 5) over the ocean, fresh-SS dominates with a concurrent decrease in biomass/biofuel burning, EC-sulfate, EC-SS and particle number concentrations. During period 6, fly ash, Ca-dust, biomass/biofuel burning, and EC-sulfate particles increased. In both cases when the HYSPLIT model shows the air mass coming from the west (Figures 3a and 3f), an increase in the fraction of fly ash particle types was detected.

[21] Figure 4b shows filter based data (24 h PM < 2.5 μm) for EC (left y axis) and sulfate and OC (right y axis) mass concentrations measured during the first half of APMEX. In general, the mass concentrations of EC and sulfate increased during the times when ATOFMS detected increased fractions of EC-sulfate and biomass/biofuel burning particles (periods 2 and 4). A corresponding decrease in the mass concentrations of EC and sulfate occurred during times when fresh-SS dominated the supermicron fraction (period 3). Increased EC-sulfate and biomass/biofuel burning fractions observed by unscaled ATOFMS data correlate with an increase in filter mass concentrations of EC and sulfate. During INDOEX similar results were observed, showing the highest levels of pollution originating from India and Southeast Asia and decreased levels from the Arabian Sea and southern Indian Ocean [*Ball et al.*, 2003; *Guazzotti et al.*, 2001, 2003; *Lobert and Harris*, 2002; *Neusüß et al.*, 2002; *Quinn et al.*, 2002; *Reiner et al.*, 2001]. Our results show that approximately 80% of EC sulfate and 84% of biomass/biofuel burning particles during APMEX were internally mixed with sulfate which suggests they underwent significant processing during transport to the sampling site.

[22] Figure 5 shows the same 6 distinct periods for submicron (0.3–1.0 μm) particles. Similar to the supermicron particles, a period with an increased fraction of submicron fly ash (15–20 October) particles was followed by a period dominated by EC-sulfate and biomass/biofuel

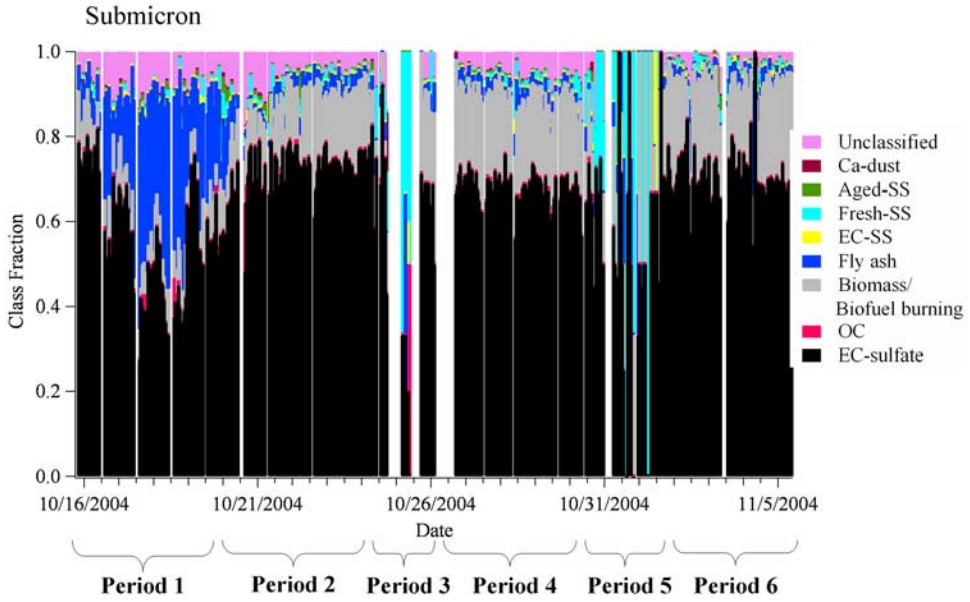

Figure 5. The fraction of submicron particle chemical classes in 1 h time resolution for the duration of the APMEX field campaign.

burning-sulfate particles (20–24 October), a period with fresh-SS (24–26 October), followed by a period with EC-sulfate and biomass/biofuel burning (26–30 October), another period of fresh-SS (30 October to 2 November), ending with a period of increasing EC-sulfate and biomass/biofuel burning number concentrations. It is important to note that ATOFMS studies in most urban areas usually detect 5–7 diverse particle types in the submicron size range, whereas in this study, just two types, EC-sulfate and biomass/biofuel burning particles, dominated the submicron aerosol as shown in Figure 5. The chemical homogeneity of the aerosol in this region suggests two possibilities: (1) a single dominating aerosol source in the region or (2) significant atmospheric processing and/or scavenging occurring during transport which converts the particles into an internally mixed homogeneous composition. Given the measured particle types and what is known about sources from previous studies, the second explanation seems to be the most likely.

[23] Aerosol measurements using the ATOFMS are subject to a number of sampling biases. Changes in shape, particle size and chemical composition have an affect on the fraction of particles that generate a mass spectrum. Irregularly shaped particles sampled into a vacuum through an aerodynamic nozzle have been shown to deviate from the aerosol beam more than spherical particles, which introduces a sampling bias against irregularly shaped particles [*Liu et al.*, 1995a, 1995b]. Most of the studies examining shape effects have been performed on an aerodynamic inlet. However, it should be noted that the ATOFMS used for APMEX used a standard converging inlet; less is known about the effects of particle shape on transmission for this inlet. It is known that this inlet does not remove water or semivolatile species, and thus most of the aged particles in this region are expected to have significant water and secondary species associated with them. The only major aerosol type during APMEX that could possibly have had a non spherical shape was EC and possibly some biomass/biofuel type [*Jiang et al.*, 2007; *Li et al.*, 2003; *Wenzel et al.*, 2003]. As we show below, these particle types were transported over a long distance across the Indian Ocean (transport time $\sim$ 2–5 days). Although fresh EC can be very non spherical, aged EC and EC at high RH has been observed to be more spherical than fresh EC [*Huang et al.*, 1994; *Spencer et al.*, 2007; *Weingartner et al.*, 1995; *Xie et al.*, 2007]. As mentioned above, the EC and biomass/biofuel burning particles also contained a significant amount of sulfate which provides further evidence that the particles were cloud processed and most likely spherical. Also, the RH during APMEX was above 70% a majority of the time. Therefore, it is likely that a shape bias for EC-sulfate and biomass/biofuel burning particles is negligible for this data set, however this could only be definitively ruled out by measuring the morphology of the aerosol directly. It is unknown whether the fly ash particles were spherical or nonspherical and there could be a shape bias that would lead to an underrepresentation of these particles based on their shape.

[24] An accurate depiction of the size distributions and number concentration for the different particle chemical classes requires use of a scaling procedure to correct for the detection bias for different particle sizes measured using ATOFMS [*Qin et al.*, 2006; *Wenzel et al.*, 2003]. To account for biases due to different particle sizes the ATOFMS data were scaled using a colocated TSI model 3321 APS. A detailed description of this scaling procedure has been reported previously and only a brief description is given here [*Qin et al.*, 2006]. The number of particles for each chemical class is divided into size and hourly bins that correspond to the same APS size and time bins. From this matrix of data the chemical classes can be scaled to the APS data. Any corrections for chemical biases can also be applied to this matrix before APS scaling.

[25] Figure 6 shows the scaled particle number concentrations for the 7 major chemical classes observed during APMEX. A correction for chemical bias is not taken into

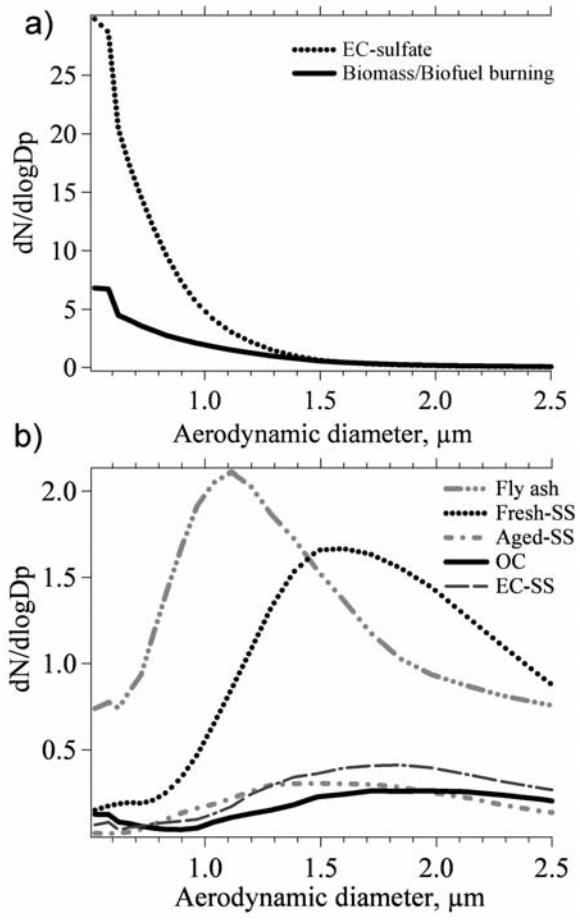

Figure 6. Scaled size distributions for the top seven chemical classes measured during APMEX.

account for these distributions because the concentrations represent an average for the entire field campaign. The size distribution for the Ca particle class is not shown because of the low number concentrations observed during the study. Figure 6a shows that the size distributions for biomass/biofuel burning and EC-sulfate particles have a steep increase in number concentration below 1 μm as would be expected for combustion particles [*Noble and Prather*, 1996]. Figure 6b shows that aged-SS, fresh-SS, SS-EC, and OC are broadly distributed with a dominant mode at $\sim$1.7 μm. As mentioned above, the OC particle type contained water. It is possible that this particle type results from a smaller organic particle that has grown to larger sizes because of the uptake of secondary species and water. Fly ash has an aerodynamic size mode centered at $\sim$1.1 μm.

[26] Figure 7a shows the time series with 1 h resolution for the particle number concentrations of particles with sizes less than 2.5 μm for the different chemical classes that have been scaled using the APS as described above. For comparison, the APS $PM_{2.5}$ number concentrations are also shown (pink line is offset by 2 units for clarity). Figure 7a has not been compensated for the fly ash and fresh sea salt chemical biases. The different colors within each hourly bar represent the number of particles for the different particle chemical classes. The six time periods discussed above are readily apparent even after scaling. Period 1 is characterized by the presence of a high abundance of supermicron Li-containing fly ash particles. In general, during periods 2 and 4 there is an increase in total particle concentrations, dominated by submicron biomass/biofuel burning and EC-sulfate particles, and a corresponding decrease in Li-containing particles. When particle concentrations were at their lowest (periods 3 and 5), supermicron sea salt particles dominated.

[27] The episodes with the "missing particle" type (possibly wet sea salt or ammonium sulfate) are shaded in green in Figure 7 (periods 4 and 6). During these time periods, the ATOFMS hit percentage was $\sim$5%. It should be noted that during the missing particle time periods, most of the missed particles had sizes above 1 μm diameter, suggesting wet sea salt was most likely responsible for the lower hit rate. Furthermore, the scanning mobility particle sizer (SMPS) data (not shown) do not show an increased number of submicron and ultrafine particles during these periods. Out of $\sim$360 h of sampling, approximately $\sim$24 h contain significant fractions of the missing particle type. If these were nominally pure sulfate aerosols, these episodes occurred for less than 10% of the total sampling time. This observation along with the observation that sulfate is most commonly found mixed with EC and biomass/biofuel suggests that, for ground based measurements, pure sulfate aerosol, used in the IPCC report and many climate models, is not an appropriate model aerosol to use in radiative forcing calculations of the Indo-Asian haze. Using a sulfate aerosol type would result in an underprediction of the aerosol forcing in this region, as internal mixtures of sulfate and EC lead to more warming of the atmosphere. Aircraft measurements are needed to determine if this is also the case for aerosols in the upper troposphere in this region.

[28] Figure 7b shows the temporal profile for the particle classes that have been scaled using the APS, and the number of fly ash and fresh sea salt particles has been adjusted for an apparent detection bias. For comparison, the APS $PM_{2.5}$ number concentrations are also shown (pink line is offset by 2 units for clarity). In Figure 7b the number of fly ash particles detected by the ATOFMS was divided by 2.5 to compensate for overcounting. The numbers of fresh sea salt particles detected by the ATOFMS were multiplied by 6 times to compensate for their apparent undercounting. Although these particles have been adjusted for their apparent biases, Figure 7b is not drastically different from Figure 7a. More specifically, adjusting fly ash and sea salt for their apparent sampling bias does not change the scaled particle number concentrations very much. This is because particles predominately in the submicron size range (such as biomass/biofuel burning and EC-sulfate) must be scaled by up to 2 orders of magnitude more compared to supermicron particles due to the size bias. Therefore small compensating changes to ATOFMS supermicron particle counts due to a detection bias have only a small effect on the number concentration (0.5–2.5 μ) due to the order of magnitudes larger number of submicron particles.

[29] Figure 8 shows a temporal plot of the absorbance (b_{ab}) measured with an aethalometer at 880 nm (left y axis) and the scattering coefficient (b_{sp}) measured with a nephelometer at 550 nm (right y axis). Both the absorbance and scattering increase during periods 2 and 4; as discussed, these are long-range transport periods from southern India.

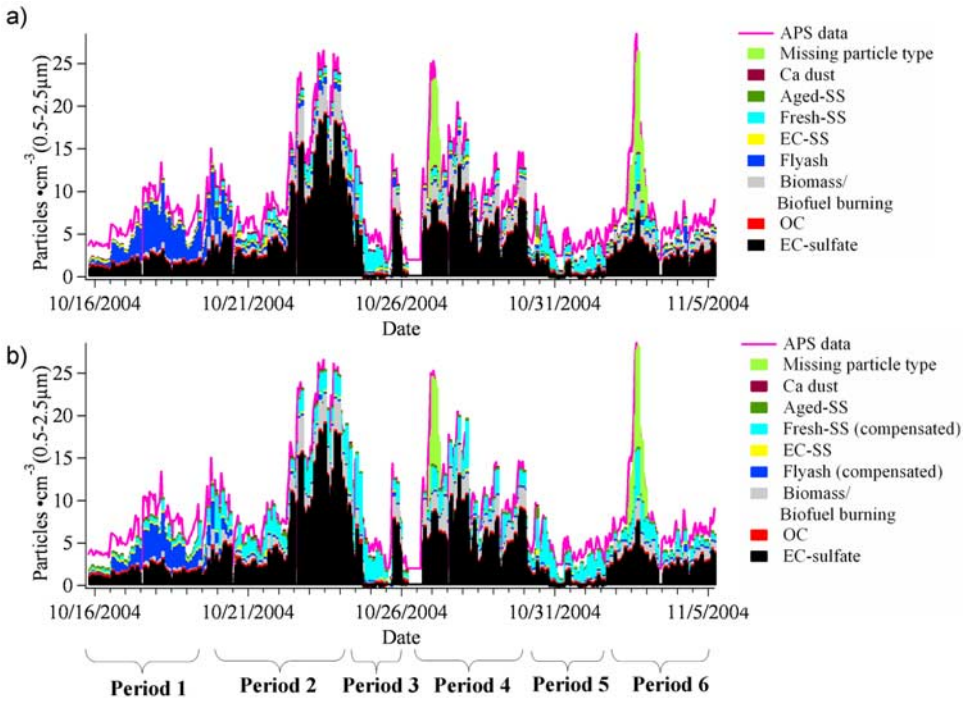

Figure 7. (a) Temporal profile for the scaled particle number concentrations for the eight chemical classes measured during APMEX. The missing particle type periods are shown in bright green. Each color represents the number of particles for a given particle type. For comparison, the total particle concentration < 2.5 μm as measured by an APS is plotted as the pink line (offset by 2 units for clarity). (b) Temporal profile for the scaled particle number concentrations after compensating for an overcounting of fly ash particles by 2.5 times and a undercounting of fresh-SS particles by 6 times.

Figure 8 also shows that during the two episodes with the missing particle types, there was a sharp increase in scattering with a corresponding decrease in the absorption of the aerosol. This is completely consistent with the ATOFMS scattering light from these particles but not absorbing UV light and producing mass spectra.

[30] *Roden et al.* [2006] report that biofuel burning from cook stoves (which is common in India) leads to a larger EC fraction than open vegetative burning. Notably, during long-range transport periods (periods 2 and 4) when the highest BC concentrations were measured with the aethalometer, 73% of the submicron particles were classified as EC-sulfate, 77% of the submicron particles contain an intense $^{39}K^{+}$ ion which is a known tracer for biomass and biofuel particles, and 71% of the EC-sulfate particles also had a large $^{39}K^{+}$ signal associated with them. Similarly, Guazzotti et al. have reported that during INDOEX a significant fraction (75%) of the particles transported from India were from a biomass/biofuel source [*Guazzotti et al.*, 2003]. Figure 9 shows the strong correlation observed between the hourly biomass/biofuel burning and EC-sulfate particle counts (R^2 = 0.92) for the entire study. This is further evidence that biofuel

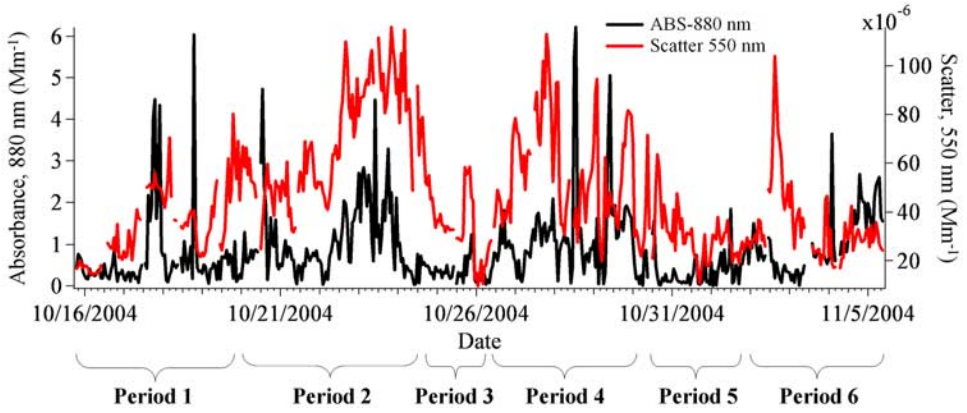

Figure 8. Aethalometer absorption coefficient (black line) is plotted on the left *y* axis, and nephelometer scattering coefficient (red line) is plotted on the right *y* axis for the duration of APMEX.

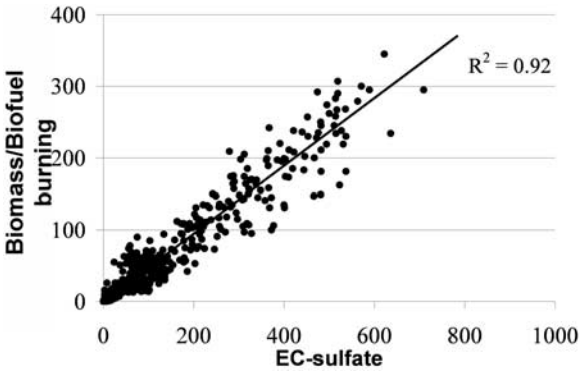

Figure 9. Correlation between the number of biomass/biofuel burning and EC-sulfate particles measured each hour during APMEX.

burning is a significant source of the EC-sulfate particles that were measured. A similar correlation ($R^2 = 0.93$) was observed by [*Stone et al.*, 2007] between mass concentrations of EC and water soluble K-containing particles.

[31] There is an interesting contrast in source contributions when the air masses were coming from the Indian (periods 2 and 4) versus Arabian (period 1) regions. A similar observation was made previously by *Guazzotti et al.* [2003]. All periods show a high fraction of K-containing particles, however, when the air mass comes from India ~75% of EC/soot is combined with K, which is indicative of biofuel signatures. In contrast, when the air mass comes from the Arabian peninsula, a large majority of K-containing particles are combined with Li^+ and other inorganic metal ions, a source signature for coal combustion or fly ash particles. Single particle mass spectral signatures are a powerful tool to distinguish between different sources with common overlapping marker ions such as potassium.

4. Conclusion

[32] During the monsoonal transition period, Hanimaadhoo experienced changes in the relative fraction and total number concentrations for different particle types that can be correlated with the direction and origin of the arriving air masses. When the air mass comes from the north and northeast from India and Sri Lanka, biofuel/biomass particles represent a significant fraction of the supermicron and submicron particles at Hanimaadhoo. When the air mass shifts to an easterly or southerly direction, a significant decrease in total particle concentrations and number of EC-sulfate and biomass/biofuel burning particles occurs with a corresponding increase in the fraction of fresh-SS. When the air mass comes from a westerly direction, Hanimaadhoo experiences an influx of supermicron and submicron fly ash type particles, possibly transported from the Arabian or African regions.

[33] In order to develop proper control strategies for the aerosols that have the largest impact on direct forcing, we must better understand the sources and processing of the aerosols in the region of the atmospheric brown cloud. The single particle mixing state of biomass/biofuel burning and elemental carbon particles in this region provides some insight into the major sources. During APMEX, biomass/biofuel burning accounts for ~75% of the EC/soot and overall particle number concentrations when the air mass originated from southern India. In contrast, when the air originated from the Arabian region, a high fraction (55%) of Li-dust or fly ash particles were detected. Similar contrasting source contributions were reported by our group previously during INDOEX in 1999 for this region [*Guazzotti et al.*, 2003]. The measured biomass/biofuel burning and EC particles contained more sulfate than freshly emitted EC (from vehicles) and biomass/biofuel burning, showing these particles have undergone extensive secondary processing. Correspondingly, during long-range transport from southern India, a larger fraction of EC mixed with sea salt was observed which also suggests EC has been cloud processed with sea salt. Interestingly, nominally pure submicron organic particles and particles containing significant amounts of nitrate which are normally observed with ATOFMS in urban environments were not observed during the long-range transport periods from India. This is possibly due to the high VOC/NO_x emission from the major combustion sources in India (i.e., two stroke engines), selective scavenging by clouds or rain during transport, or a lack of photochemistry and ozone in this region (as discussed above). The hygroscopic properties of EC particles transported from India and Sri Lanka to Hanimaadhoo increased due to the fact that the particles have become internally mixed with secondary sulfate during transport. Furthermore, the light absorption by carbonaceous particles transported over the Indian Ocean from India and Sri Lanka could be significantly enhanced if sulfate and NaCl exist as shells surrounding an absorbing EC core. The observed single particle mixing of sulfate with biomass/biofuel and EC/soot particles can thus at least partly explain the large solar heating observed during INDOEX [*Ramanathan et al.*, 2001] of atmospheric brown clouds. Biomass/biofuel burning and EC particles transported from India and Sri Lanka over the Indian Ocean should be represented as being internally mixed with sulfate in climate models for the region. Future studies will calculate the forcing of the aerosol in this region using the measured size-resolved single particle mixing state of aerosols.

[34] **Acknowledgments.** Filter data were kindly made available by James Schauer and Elizabeth Stone from University of Wisconsin–Madison. Financial support for this research was given by the Atmospheric Brown Cloud project funded under the United Nations Environmental Programme and NOAA.

References

Alfaro, S. C., A. Gaudichet, J. L. Rajot, L. Gomes, M. Maillé, and H. Cachier (2003), Variability of aerosol size-resolved composition at an Indian coastal site during the Indian Ocean Experiment (INDOEX) intensive field phase, *J. Geophys. Res.*, *108*(D8), 4235, doi:10.1029/2002JD002645.

Anderson, T. L., and J. A. Ogren (1998), Determining aerosol radiative properties using the TSI 3563 integrating nephelometer, *Aerosol Sci. Technol.*, *29*(1), 57–69.

Arnott, W. P., K. Hamasha, H. Moosmuller, P. J. Sheridan, and J. A. Ogren (2005), Towards aerosol light-absorption measurements with a 7-wavelength aethalometer: Evaluation with a photoacoustic instrument and 3-wavelength nephelometer, *Aerosol Sci. Technol.*, *39*(1), 17–29.

Ball, W. P., R. R. Dickerson, B. G. Doddridge, J. W. Stehr, T. L. Miller, D. L. Savoie, and T. P. Carsey (2003), Bulk and size-segregated aerosol composition observed during INDOEX 1999: Overview of meteorology and continental impacts, *J. Geophys. Res.*, *108*(D10), 8001, doi:10.1029/2002JD002467.

Bond, T. C., G. Habib, and R. W. Bergstrom (2006), Limitations in the enhancement of visible light absorption due to mixing state, *J. Geophys. Res.*, *111*, D20211, doi:10.1029/2006JD007315.

Chandra, S., S. K. Satheesh, and J. Srinivasan (2004), Can the state of mixing of black carbon aerosols explain the mystery of 'excess' atmospheric absorption?, *Geophys. Res. Lett.*, *31*, L19109, doi:10.1029/2004GL020662.

Chen, Y., and J. E. Penner (2005), Uncertainty analysis for estimates of the first indirect aerosol effect, *Atmos. Chem. Phys.*, *5*, 2935–2948.

Clarke, A. D., et al. (2004), Size distributions and mixtures of dust and black carbon aerosol in Asian outflow: Physiochemistry and optical properties, *J. Geophys. Res.*, *109*, D15S09, doi:10.1029/2003JD004378.

Corrigan, C. E., V. Ramanathan, and J. J. Schauer (2006), Impact of monsoon transitions on the physical and optical properties of aerosols, *J. Geophys. Res.*, *111*, D18208, doi:10.1029/2005JD006370.

Debaje, S. B., S. J. Jeyakumar, K. Ganesan, D. B. Jadhav, and P. Seetaramayya (2003), Surface ozone measurements at tropical rural coastal station Tranquebar, India, *Atmos. Environ.*, *37*(35), 4911–4916.

Dickerson, R. R., M. O. Andreae, T. Campos, O. L. Mayol-Bracero, C. Neusuess, and D. G. Streets (2002), Analysis of black carbon and carbon monoxide observed over the Indian Ocean: Implications for emissions and photochemistry, *J. Geophys. Res.*, *107*(D19), 8017, doi:10.1029/2001JD000501.

Dusek, U., G. P. Reischl, and R. Hitzenberger (2006), CCN activation of pure and coated carbon black particles, *Environ. Sci. Technol.*, *40*(4), 1223–1230.

Fuller, K. A., W. C. Malm, and S. M. Kreidenweis (1999), Effects of mixing on extinction by carbonaceous particles, *J. Geophys. Res.*, *104*(D13), 15,941–15,954.

Gard, E., J. E. Mayer, B. D. Morrical, T. Dienes, D. P. Fergenson, and K. A. Prather (1997), Real-time analysis of individual atmospheric aerosol particles: Design and performance of a portable ATOFMS, *Anal. Chem.*, *69*(20), 4083–4091.

Guazzotti, S. A., K. R. Coffee, and K. A. Prather (2001), Continuous measurements of size-resolved particle chemistry during INDOEX-intensive field phase 99, *J. Geophys. Res.*, *106*(D22), 28,607–28,627.

Guazzotti, S. A., et al. (2003), Characterization of carbonaceous aerosols outflow from India and Arabia: Biomass/biofuel burning and fossil fuel combustion, *J. Geophys. Res.*, *108*(D15), 4485, doi:10.1029/2002JD003277.

Hopke, P. K., and X. H. Song (1997), Classification of single particles by neural networks based on the computer-controlled scanning electron microscopy data, *Anal. Chim. Acta*, *348*(1–3), 375–388.

Huang, P. F., B. J. Turpin, M. J. Pipho, D. B. Kittelson, and P. H. McMurry (1994), Effects of water condensation and evaporation on diesel chain-agglomerate morphology, *J. Aerosol Sci.*, *25*(3), 447–459.

Intergovernmental Panel on Climate Change (2001), *Climate Change 2001: The Scientific Basis—Contribution of Working Group I to the Third Assessment Report of the Intergovernmental Panel on Climate Change*, Cambridge Univ. Press, New York.

Jacobson, M. Z. (2001), Strong radiative heating due to the mixing state of black carbon in atmospheric aerosols, *Nature*, *409*(6821), 695–697.

Jiang, J. G., X. Xu, J. Wang, S. J. Yang, and Y. Zhang (2007), Investigation of basic properties of fly ash from urban waste incinerators in China, *J. Environ. Sci. China*, *19*(4), 458–463.

Kaneyasu, N., and S. Murayama (2000), High concentrations of black carbon over middle latitudes in the north Pacific Ocean, *J. Geophys. Res.*, *105*(D15), 19,881–19,890.

Knutti, R., T. F. Stocker, F. Joos, and G. K. Plattner (2002), Constraints on radiative forcing and future climate change from observations and climate model ensembles, *Nature*, *416*(6882), 719–723.

Kripalani, R. H., and P. Kumar (2004), Northeast monsoon rainfall variability over south peninsular India vis-a-vis the Indian Ocean dipole mode, *Int. J. Climatol.*, *24*(10), 1267–1282.

Lal, S., M. Naja, and B. H. Subbaraya (2000), Seasonal variations in surface ozone and its precursors over an urban site in India, *Atmos. Environ.*, *34*(17), 2713–2724.

Li, J., M. Pósfai, P. V. Hobbs, and P. R. Buseck (2003), Individual aerosol particles from biomass burning in southern Africa: 2, Compositions and aging of inorganic particles, *J. Geophys. Res.*, *108*(D13), 8484, doi:10.1029/2002JD002310.

Liu, P., P. J. Ziemann, D. B. Kittelson, and P. H. McMurry (1995a), Generating particle beams of controlled dimensions and divergence 1: Theory of particle motion in aerodynamic lenses and nozzle expansions, *Aerosol Sci. Technol.*, *22*(3), 293–313.

Liu, P., P. J. Ziemann, D. B. Kittelson, and P. H. McMurry (1995b), Generating particle beams of controlled dimensions and divergence 2: Experimental evaluation of particle motion in aerodynamic lenses and nozzle expansions, *Aerosol Sci. Technol.*, *22*(3), 314–324.

Lobert, J. M., and J. M. Harris (2002), Trace gases and air mass origin at Kaashidhoo, Indian Ocean, *J. Geophys. Res.*, *107*(D19), 8013, doi:10.1029/2001JD000731.

Lohmann, U., and J. Feichter (2005), Global indirect aerosol effects: A review, *Atmos. Chem. Phys.*, *5*, 715–737.

Moffet, R. C., and K. A. Prather (2005), Extending ATOFMS measurements to include refractive index and density, *Anal. Chem.*, *77*(20), 6535–6541.

Morgan, M. G., P. J. Adams, and D. W. Keith (2006), Elicitation of expert judgments of aerosol forcing, *Clim. Change*, *75*(1–2), 195–214.

Myhre, G., F. Stordal, T. F. Berglen, J. K. Sundet, and I. S. A. Isaksen (2004), Uncertainties in the radiative forcing due to sulfate aerosols, *J. Atmos. Sci.*, *61*(5), 485–498.

Neusüß, C., T. Gnauk, A. Plewka, H. Herrmann, and P. K. Quinn (2002), Carbonaceous aerosol over the Indian Ocean: OC/EC fractions and selected specifications from size-segregated onboard samples, *J. Geophys. Res.*, *107*(D19), 8031, doi:10.1029/2001JD000327.

Noble, C. A., and K. A. Prather (1996), Real-time measurement of correlated size and composition profiles of individual atmospheric aerosol particles, *Environ. Sci. Technol.*, *30*(9), 2667–2680.

Prather, K. A., T. Nordmeyer, and K. Salt (1994), Real-time characterization of individual aerosol particles using time-of-flight mass spectrometry, *Anal. Chem.*, *66*(9), 1403–1407.

Qin, X. Y., P. V. Bhave, and K. A. Prather (2006), Comparison of two methods for obtaining quantitative mass concentrations from aerosol time-of-flight mass spectrometry measurements, *Anal. Chem.*, *78*(17), 6169–6178.

Quinn, P. K., D. J. Coffman, T. S. Bates, T. L. Miller, J. E. Johnson, E. J. Welton, C. Neusüss, M. Miller, and P. J. Sheridan (2002), Aerosol optical properties during INDOEX 1999: Means, variability, and controlling factors, *J. Geophys. Res.*, *107*(D19), 8020, doi:10.1029/2000JD000037.

Ramana, M. V., and V. Ramanathan (2006), Abrupt transition from natural to anthropogenic aerosol radiative forcing: Observations at the ABC-Maldives Climate Observatory, *J. Geophys. Res.*, *111*, D20207, doi:10.1029/2006JD007063.

Ramanathan, V., et al. (2001), Indian ocean experiment: An integrated analysis of the climate forcing and effects of the great Indo-Asian haze, *J. Geophys. Res.*, *106*(D22), 28,371–28,398.

Ramanathan, V., C. Chung, D. Kim, T. Bettge, L. Buja, J. T. Kiehl, W. M. Washington, Q. Fu, D. R. Sikka, and M. Wild (2005), Atmospheric brown clouds: Impacts on south Asian climate and hydrological cycle, *Proc. Natl. Acad. Sci. U. S. A.*, *102*(15), 5326–5333.

Rebotier, T. P., and K. A. Prather (2007), Aerosol time-of-flight mass spectrometry data analysis: A benchmark of clustering algorithms, *Anal. Chim. Acta*, *585*(1), 38–54.

Reiner, T., D. Sprung, C. Jost, R. Gabriel, O. L. Mayol-Bracero, M. O. Andreae, T. L. Campos, and R. E. Shetter (2001), Chemical characterization of pollution layers over the tropical Indian ocean: Signatures of emissions from biomass and fossil fuel burning, *J. Geophys. Res.*, *106*(D22), 28,497–28,510.

Roden, C. A., T. C. Bond, S. Conway, A. Benjamin, and O. Pinel (2006), Emission factors and real-time optical properties of particles emitted from traditional wood burning cookstoves, *Environ. Sci. Technol.*, *40*(21), 6750–6757.

Schnaiter, M., C. Linke, O. Möhler, K.-H. Naumann, H. Saathoff, R. Wagner, U. Schurath, and B. Wehner (2005), Absorption amplification of black carbon internally mixed with secondary organic aerosol, *J. Geophys. Res.*, *110*, D19204, doi:10.1029/2005JD006046.

Schwartz, S. E. (2004), Uncertainty requirements in radiative forcing of climate change, *J. Air Waste Manage. Assoc.*, *54*(11), 1351–1359.

Silva, P. J., D.-Y. Liu, C. A. Noble, and K. A. Prather (1999), Size and chemical characterization of individual particles resulting from biomass burning of local southern California species, *Environ. Sci. Technol.*, *33*(18), 3068–3076.

Sodeman, D. A., S. M. Toner, and K. A. Prather (2005), Determination of single particle mass spectral signatures from light duty vehicle emissions, *Environ. Sci. Technol.*, *39*(12), 4569–4580.

Song, X.-H., P. K. Hopke, D. P. Fergenson, and K. A. Prather (1999), Classification of single particles analyzed by ATOFMS using an artificial neural network, ART-2a, *Anal. Chem.*, *71*(4), 860–865.

Spencer, M. T., L. G. Shields, and K. A. Prather (2007), Simultaneous measurement of the effective density and chemical composition of ambient aerosol particles, *Environ. Sci. Technol.*, *41*(4), 1303–1309.

Stehr, J. W., W. P. Ball, R. R. Dickerson, B. G. Doddridge, C. A. Piety, and J. E. Johnson (2002), Latitudinal gradients in O_3 and CO during INDOEX 1999, *J. Geophys. Res.*, *107*(D19), 8016, doi:10.1029/2001JD000446.

Stier, P., J. H. Seinfeld, S. Kinne, J. Feichter, and O. Boucher (2006), Impact of nonabsorbing anthropogenic aerosols on clear-sky atmospheric absorption, *J. Geophys. Res.*, *111*, D18201, doi:10.1029/2006JD007147.

Stone, E. A., G. C. Lough, J. J. Schauer, P. S. Praveen, C. E. Corrigan, and V. Ramanathan (2007), Understanding the origin of black carbon in the atmospheric brown cloud over the Indian Ocean, *J. Geophys. Res.*, *112*, D22S23, doi:10.1029/2006JD008118.

Suess, D. T. (2002), Single particle mass spectrometry combustion source characterization and atmospheric apportionment of vehicular, coal, and biofuel exhaust emissions, Ph.D. thesis, Univ. of Calif., Riverside.

Thomson, D. S., A. M. Middlebrook, and D. M. Murphy (1997), Thresholds for laser-induced ion formation from aerosols in a vacuum using ultraviolet and vacuum-ultraviolet laser wavelengths, *Aerosol Sci. Technol.*, *26*(6), 544–559.

Toner, S. M., D. A. Sodeman, and K. A. Prather (2006), Single particle characterization of ultrafine and accumulation mode particles from heavy duty diesel vehicles using aerosol time-of-flight mass spectrometry, *Environ. Sci. Technol.*, *40*(12), 3912–3921.

Vijayan, V., S. N. Behera, V. S. Ramamurthy, S. Puri, J. S. Shahi, and N. Singh (1997), Elemental composition of fly ash from a coal-fired thermal power plant: A study using PIXE and EDXRF, *X Ray Spectrom.*, *26*(2), 65–68.

Weingartner, E., U. Baltensperger, and H. Burtscher (1995), Growth and structural-change of combustion aerosols at high relative-humidity, *Environ. Sci. Technol.*, *29*(12), 2982–2986.

Wentzel, M., H. Gorzawski, K. H. Naumann, H. Saathoff, and S. Weinbruch (2003), Transmission electron microscopical and aerosol dynamical characterization of soot aerosols, *J. Aerosol Sci.*, *34*(10), 1347–1370.

Wenzel, R. J., D. Liu, E. S. Edgerton, and K. A. Prather (2003), Aerosol time-of-flight mass spectrometry during the Atlanta Supersite Experiment: 2. Scaling procedures, *J. Geophys. Res.*, *108*(D7), 8427, doi:10.1029/2001JD001563.

Xie, Z., J. D. Blum, S. Utsunomiya, R. C. Ewing, X. Wang, and L. Sun (2007), Summertime carbonaceous aerosols collected in the marine boundary layer of the Arctic Ocean, *J. Geophys. Res.*, *112*, D02306, doi:10.1029/2006JD007247.

Zhang, C. F., Y. Qiang, and J. M. Sun (2005), Characteristics of particulate matter from emissions of four typical coal-fired power plants in China, *Fuel Processing Technol.*, *86*(7), 757–768.

C. E. Corrigan, J. C. Holecek, and V. Ramanathan, Center for Atmospheric Sciences, Scripps Institution of Oceanography, University of California, San Diego, La Jolla, CA 92093, USA.

K. A. Prather and M. T. Spencer, Department of Chemistry and Biochemistry, University of California, San Diego, La Jolla, CA 92093, USA. (kprather@ucsd.edu)